Models of Electrical Activity: Calibration and Prediction Testing on the Same Cell

Maurizio Tomaiuolo,[†] Richard Bertram,[‡]* Gareth Leng,[§] and Joël Tabak[†]
[†]Department of Biological Science and Program in Neuroscience, Florida State University, Tallahassee, Florida; [‡]Department of Mathematics and Programs in Neuroscience and Molecular Biophysics, Florida State University, Tallahassee, Florida; and [§]Centre for Integrative Physiology, University of Edinburgh, Edinburgh, United Kingdom

ABSTRACT   Mathematical models are increasingly important in biology, and testability is becoming a critical issue. One limitation is that one model simulation tests a parameter set representing one instance of the biological counterpart, whereas biological systems are heterogeneous in their properties and behavior, and a model often is fitted to represent an ideal average. This is also true for models of a cell's electrical activity; even within a narrowly defined population there can be considerable variation in electrophysiological phenotype. Here, we describe a computational experimental approach for parameterizing a model of the electrical activity of a cell in real time. We combine the inexpensive parallel computational power of a programmable graphics processing unit with the flexibility of the dynamic clamp method. The approach involves 1), recording a cell's electrical activity, 2), parameterizing a model to the recording, 3), generating predictions, and 4), testing the predictions on the same cell used for the calibration. We demonstrate the experimental feasibility of our approach using a cell line (GH4C1). These cells are electrically active, and they display tonic spiking or bursting. We use our approach to predict parameter changes that can convert one pattern to the other.

INTRODUCTION

Mathematical models have become essential tools for understanding complex biological systems. Models are used to formulate hypotheses that can be tested through simulations and can generate new predictions that will in turn be tested experimentally. One limitation of this process is that simulations only test one set of parameter values, whereas biological systems such as cells often form heterogeneous populations, so a single parameter set may not be representative of many of the individuals in a population. However narrowly we try to define a cell population, it seems that substantial heterogeneity remains. For example, pituitary lactotrophs exhibit significant heterogeneity in calcium influx and electrophysiological characteristics (1–3), even within functional subtypes (4). When different parameters are measured in different cells and then averaged, this can lead to an average model that may represent only a subpopulation of cells or, in the worst case, none at all. The behavior of the average model may not represent the average behavior in the cell population (5–7).

One way to overcome this problem is to use tools of dynamical systems theory, such as bifurcation diagrams, to obtain a qualitative understanding of how the system's dynamics change as parameters are varied (8). A second approach, akin to sensitivity analysis, is to simulate thousands or millions of models built from different parameter combinations, to understand how groups of parameters can compensate each other's variations and produce a given behavior (9,10). Although these approaches have provided great insight into biological systems, neither provides an accurate mechanistic description of single individuals in a population.

An ideal scenario would be to measure a cell's activity, build a dynamical model of that cell, and then test the model's predictions on the same cell. Only then might we be able to fully understand how differences in parameter values translate into differences in cell behavior.

Here, we consider anterior pituitary cells that spontaneously produce patterns of electrical activity. Pituitary lactotrophs and somatotrophs spontaneously generate patterns of Ca^{2+}-dependent spikes and bursts. Bursts create large intracellular Ca^{2+} transients that are thought to underlie basal hormone secretion (11). We use the GH4C1 lactosomatotroph cell line. These cells generate spiking or bursting activity patterns, with large cell-to-cell variations in electrical activity. What differences in parameters, such as ion channel conductances, underlie the differences in electrical activity patterns? To answer this question, we have developed an approach for testing models of electrical activity on the same cells used to calibrate the model. To do so, we used the parallel processing capability of a programmable graphics processing unit (GPU) that is available at a low cost, and the flexibility of the dynamic-clamp protocol (12,13).

In the following sections, we first show that a simply built model whose electrical activity qualitatively matches spontaneous experimental activity cannot always be used to generate useful predictions, a point demonstrated experimentally in an invertebrate central pattern generator (14). We then describe the strategy used to estimate the parameters of our model and use synthetic data to explore the relationship between the fitness of the best-fit model and the

proximity of its parameters to those of the model used to generate the data. It is important to note that we test the ability of the best-fit model to generate qualitative predictions when some parameters are set to an incorrect value or one conductance is missing from the model. Finally, we test the procedure on actual cells. We first record spontaneous activity from a cell, from which we extract features that the model must reproduce. We also measure whole-cell currents generated in response to voltage steps. From this information, we estimate a subset of the parameters of our model of pituitary electrical activity.

The computational speed of the GPU allows the estimation process to be completed in 10 min. Therefore, the vast majority of the cells we record from are still healthy at the end of the calibration and can be used to test model predictions. We show how fits obtained from spiking and bursting cells can be used to predict parameter changes that can switch the electrical activity pattern from spiking to bursting, or vice versa. We then perform such parameter changes experimentally, using the dynamic-clamp technique on the same cells that were used to calibrate the model. Despite the simplicity of our model, we show that it can generate novel predictions that can be tested directly. Thus, we demonstrate that the combination of mathematical modeling, fast parallel processing provided by a GPU, and the dynamic-clamp technique can overcome modeling limitations due to cell heterogeneity.

MATERIALS AND METHODS

Mathematical model

We use a previously developed mathematical model for the electrical activity and Ca^{2+} handling in a pituitary lactotroph [15]. It consists of voltage-gated Ca^{2+} and K^+ currents (I_{Ca} and I_K, respectively) for the production of action potentials, a leak current, and a Ca^{2+}-activated K^+ current (I_{SK}, a small-conductance K(Ca) current). A voltage-dependent current through large-conductance K^+ channels (BK channels) is also included. Although these BK channels are both voltage- and Ca^{2+}-gated, they are typically located adjacent to Ca^{2+} channels and are gated by Ca^{2+} nanodomains [16]. Because the Ca^{2+} concentration sensed by the BK channel reaches equilibrium in microseconds, the activation can be modeled as a purely voltage-dependent process [17,18]. The following equations describe the dynamics of the model variables V (membrane potential), n (activation of I_K), b (activation of I_{BK}) and [Ca] (intracellular Ca^{2+} concentration):

$$C_m \frac{dV}{dt} = -(I_{Ca} + I_K + I_{SK} + I_{BK} + I_{leak}), \quad (1)$$

$$\tau_n \frac{dn}{dt} = n_\infty(V) - n, \quad (2)$$

$$\tau_{BK} \frac{db}{dt} = b_\infty(V) - b, \quad (3)$$

$$\frac{d[Ca]}{dt} = -f_c(\alpha I_{Ca} + k_c[Ca]), \quad (4)$$

with ionic currents $I_{Ca} = g_{Ca}m_\infty(V)(V - V_{Ca})$, $I_K = g_K n(V - V_K)$, $I_{SK} = g_{SK} s_\infty([Ca])(V - V_K)$, $I_{BK} = g_{BK} b(V - V_K)$, and $I_{leak} = g_{leak}(V - V_{leak})$, and steady-state functions $m_\infty(V) = [1 + exp((v_m - V)/s_m)]^{-1}$, $n_\infty(V) = [1 + exp((v_n - V)/s_n)]^{-1}$, $s_\infty([Ca]) = [Ca]^2/[Ca]^2 + k_s^2$, and $b_\infty(V) = [1 + exp((v_b - V)/s_b)]^{-1}$.

Default parameter values are given in Table 1. Most simulations were run on a GPU using custom code. The simulation package XPPAUT [19] was used to run single instances of the model (forward Euler method, dt = 0.005 ms). Computer codes for this model are freely available at www.math.fsu.edu/~bertram/software/pituitary.

Feature-based fitness function

We used features of the recorded electrical activity trace to create a fitness function that is optimized to calibrate model parameters [20]. First we select a voltage trace (usually a few minutes of electrical activity) and then extract features that represent its shape. The features used in this study were the minimum voltage achieved during the trace, the difference between the minimum and the maximum (amplitude), the period of the oscillation (either spiking or bursting), and the ratio of the duration of the silent phase to the period. We computed a silent phase as the time within a period during which the voltage lies below a threshold $T = min(V) + 0.35(max(V) - min(V))$. For bursting cases, we also used the number of peaks in a burst and the sum of the peak amplitudes as features. The fitness is computed with a Gaussian distance function that uses the extracted features as targets or optima. The fitness of a model is then

$$w = \frac{\sum_j c_j \, exp\left(-\frac{(f_j - opt_j)^2}{\sigma_j}\right)}{\sum_j c_j}, \quad (5)$$

where c_j represents the contribution of feature j to the overall fitness, f_j and opt_j are the computed and target features, respectively, and σ_j is the reciprocal strength of selection on that feature (small values represent strong selection). The sum in the denominator scales the computed fitness between 0 and 1. A value of 1 indicates a complete agreement between the features extracted from the target voltage trace and those extracted from the best-fit trace. For all simulations, the values used for the fitness coefficients, c, and selection strengths, σ, were min(V), $c = 2$ and $\sigma = 10$ mV^2; amplitude, $c = 2$ and $\sigma = 10$ mV^2; period, $c = 4$ and $\sigma = 50$ ms^2; silent/period ratio, $c = 2$ and $\sigma = 0.025$; burst-peak number, $c = 1$ and $\sigma = 1$; burst-peak amplitude, $c = 1$ and $\sigma = 1$ mV^2.

With voltage-clamp data, the fitness function was modified to

$$w = \beta w_{features} + (1 - \beta)w_{clamp}, \quad (6)$$

with

$$RMSE = \sum_i \sqrt{\frac{(I_{i,model} - I_{i,cell})^2}{kr}}, \quad (7)$$

and

$$w_{clamp} = exp\left(\frac{-RMSE^2}{\sigma_{clamp}}\right), \quad (8)$$

where the summation is over the number of different test potentials, $I_{i,model}$ and $I_{i,cell}$ are equilibrium currents in the model and the cell, respectively, and the rescaling constant kr is 1 pA^2. Parameter β is between 0 and 1 and adjusts the relative weight given to features versus

TABLE 1   Parameter values used in the simulations, unless otherwise noted

Parameter	Min	Default value	Max	Definition
C	5	10 pF	15	Membrane capacitance
g_{Ca}	0.5	2 nS	5	Maximal conductance of Ca^{2+} channels
V_{Ca}		60 mV		Reversal potential for Ca^{2+}
v_m	-30	-20 mV	-10	Voltage value at midpoint of m_∞
s_m	2	12 mV	24	Slope parameter of m_∞
g_K	0.5	4 nS	8	Maximal conductance of K channels
V_K		-75 mV		Reversal potential for K^+
v_n	-10	-5 mV	-1	Voltage value at midpoint of n_∞
s_n	2	10 mV	20	Slope parameter of n_∞
τ_n	10	20 ms	30	Time constant of n
g_{SK}	0.5	2 nS	6	Maximal conductance of SK channels
k_s	0.1	0.4 μM	1	[Ca] at midpoint of s_∞
g_{BK}	0	0.1 or 0.8 nS	4	Maximal conductance of BK channels
v_b		-20 mV		Voltage value at midpoint of b_∞
s_b		2 mV		Slope parameter of b_∞
τ_b	1	5 ms	10	Time constant of b
g_{leak}	0.05	0.2 nS	0.3	Leak conductance
V_{leak}		-50 mV		Reversal potential for the leak current
g_A	0	0 nS	40	Maximal conductance of A channels
v_a		-20 mV		Voltage value at midpoint of a_∞
s_a		10 mV		Slope parameter of a_∞
v_h		-60 mV		Voltage value at midpoint of h_∞
s_h		5 mV		Slope parameter of h_∞
τ_h		20 ms		Time constant of h
f_c		0.01		Fraction of free Ca^{2+} ions in cytoplasm
α		0.0015 μMfC^{-1}		Conversion from charges to molar concentration
k_c	0.01	0.12 ms^{-1}	0.4	Rate of Ca^{2+} extrusion

voltage-clamp currents in the model calibration (we used 0.7), $\sigma_{clamp} = 500$ mV^2.

Strategy for model calibration

To calibrate the parameters of the model to match the voltage trace of a cell we developed custom software written in C# and interfaced with a programmable GPU (CUDA parallel computing architecture, NVIDIA, Santa Clara, CA) using OpenCL. The GPU can simultaneously run simulations of thousands of different individuals, corresponding to renditions of the model with different parameter combinations. The forward Euler method was used to integrate the equations with a time step of 0.005 ms. To accelerate the process we also evaluated the features of each individual using the GPU. The features were scored during the second half of the simulation, thus ensuring that transients were eliminated. Each parallel set of simulations is referred to as a generation.

We chose 4096 initial sets of parameters using a Latin hypercube sampling scheme (21), a statistical method to generate a distribution of parameter values from a multidimensional distribution. The parameter ranges used to generate the initial distribution are given in Table 1. Each individual model is simulated for 10 s of electrical activity and receives a fitness score. The best 32 models are used for the next generation. We use these 32 parameter combinations to form 32 blocks of models. The parameter sets for the next generation are generated by creating 128 replicates of each model in each block. We leave one replicate unchanged and mutate the other replicates. This guarantees that we always carry the best 32 parameter combinations to the next generation. The size of a mutation was randomly drawn according to a normal distribution centered at the value of each parameter and with standard deviation σ (we used 0.1). Altogether, this forms $128 \times 32 = 4096$ model cells. Setting parameters, simulating, and scoring each model takes a little more than 1 min/generation (using an NVIDIA GeForce GTX 560 GPU), and typically 10 generations were sufficient to achieve a good fit.

Cell preparations and perforated patch recordings

GH4C1 cells were obtained from ATCC (Manassas, VA) and maintained in culture conditions in supplemented F10 medium (Sigma-Aldrich, St-Louis, MO) according to established procedures (22). During the experiment, cells were superfused with Hepes-buffered saline (138 mM NaCl, 5 mM KCl, 10 mM α-D-glucose, 25 mM HEPES, 0.7 mM Na$_2$HPO$_4$, 1 mM MgCl$_2$, and 2 mM CaCl$_2$) at room temperature. Fire-polished pipettes (resistance 6–9 MOhm) were filled with intracellular solution containing 90 mM KAsp, 60 mM KCl, 10 mM HEPES, 1 mM MgCl$_2$, and 120 μg/ml amphotericin B. Access resistance usually decreased to <50 MΩ within 10 min after seal (>5 GΩ) formation. A junction potential of 6.5 mV was not corrected; an undischarged Donnan potential also exists across the perforated membrane, but it is assumed to be negligible. Bath application of 1 μM paxilline (Tocris, Ellisville, MO) or 100 nM iberiotoxin (Tocris) was used to block BK channels. Note that the perforated patch configuration is critical to perform parameter estimation and model testing on the same cell, because in whole-cell mode, Ca^{2+} currents responsible for electrical activity run down after a few minutes.

Dynamic clamp

Membrane potential was monitored in current clamp (bridge mode) and acquired from the patch amplifier (Multiclamp 700B, Molecular Devices, Sunnyvale, CA) through an analog-to-digital acquisition card (DAQ) on a separate PC running the software QuB with a dynamic-clamp module (23). Membrane potential (V) was used to compute the current to be injected using the same mathematical expression as for the model simulations. For example, for the BK current, we computed $I_{BK} = g_{BK} b (V - V_K)$, with b obtained by integrating Eq. 3. This calculated current was injected into the cell through the same DAQ. The equations to compute the currents were evaluated in real time using the forward Euler method (23), with an

average time step of dt $= 54$ μs, maximum $= 100$ μs, and coefficient of variation ≤ 1.2.

RESULTS

Models exhibiting similar spontaneous activity can respond very differently to conductance changes

When building a cellular model, usually we combine available experimental data (such as types of channels present on the cells and channel kinetic rates) with our intuition to produce a set of equations that matches the cell's electrical activity (such as firing rate or pattern). However, models with different parameter sets can produce similar behavior (9,24). If these parameter sets occupy different regions in parameter space, then changes in some parameters (typically the maximal conductances of the various ionic currents) may result in different qualitative changes in the electrical activity pattern. In other words, models that produce similar activity patterns often predict different changes in activity after changes in parameters (14). This is particularly relevant for pituitary cells, since the distribution and properties of ion channels vary among cell types and even within the same cell type, depending on physiological conditions. Thus two cells that exhibit a similar activity pattern might have different reactions to a change in parameters.

We illustrate this in Fig. 1. First we choose three parameter sets (Table 2) that result in tonic spiking. These sets have different values for five maximal conductances: an L-type Ca^{2+} current (g_{Ca}), a delayed-rectifying K^+ current (g_K), an SK-type K^+ current (g_{SK}), a BK-type K^+ current (g_{BK}) and a leak current (g_{leak}). A list of the remaining parameters and their values is given in Table 1 (default values). These individuals represent different electrically excitable cells, characterized by different locations in parameter space, yet all exhibit tonic spiking.

We start with model cell A (Fig. 1 A a) by increasing g_{ca} by 1 nS (Fig. 1 A b) and observing the effect. We then repeat the process with g_{BK} (Fig. 1 A c). Neither modification results in a qualitative change in the tonic spiking pattern; the spike frequency and amplitude are altered, but the spiking pattern persists. We then apply these changes to model cell B (Fig. 1 B, a–c), which has different values for the five maximal conductances listed above. In this case, increasing g_{Ca} by 1 nS again has no qualitative effect on the tonic spiking pattern, whereas increasing g_{BK} by 1 nS converts the tonic spiking pattern to a bursting pattern that is characteristic of pituitary somatotrophs (25) and lactotrophs (26). The opposite is true for model cell C (Fig. 1 C, a–c), in which increasing g_{Ca}, but not g_{BK}, results in a change from tonic spiking to bursting.

This example illustrates how cells producing similar spiking patterns can behave very differently in response to
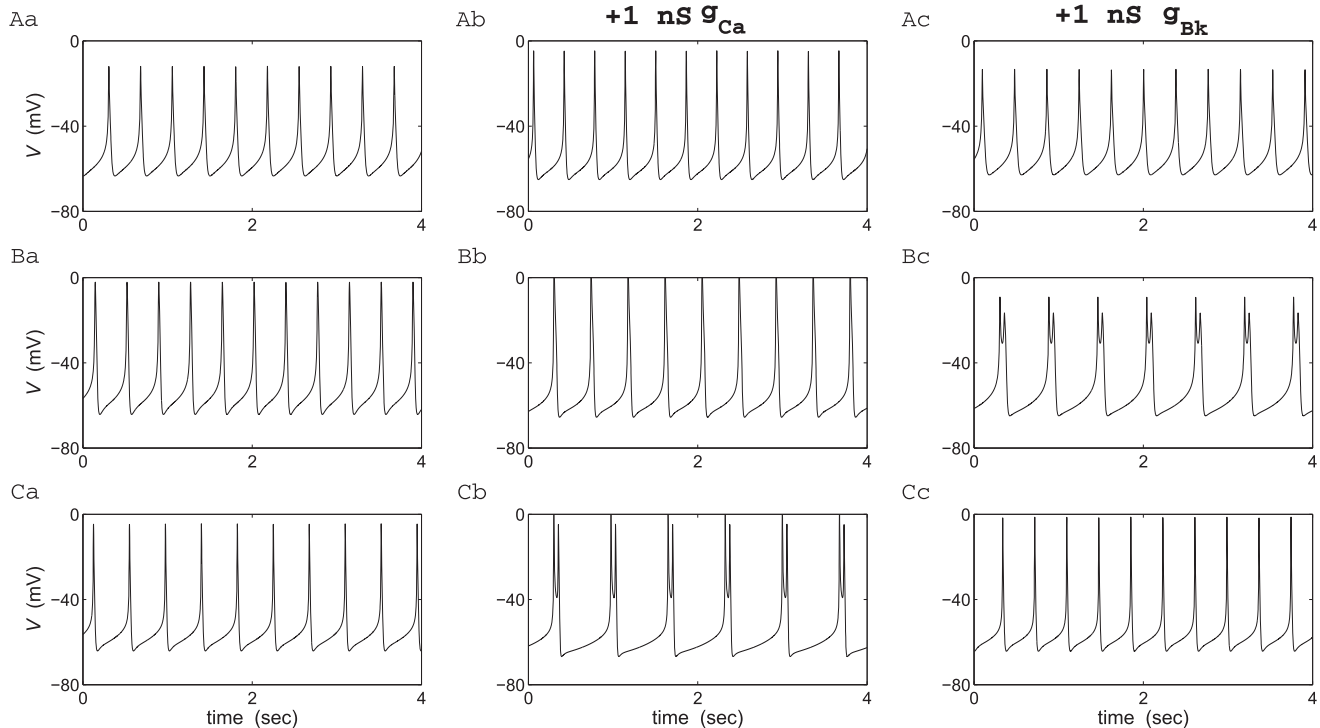

FIGURE 1 Model calibration is important for reliable predictions. Three different combinations of the conductances g_{Ca}, g_K, g_{SK}, g_{BK}, and g_{leak} are used in the model (Table 2), with each combination producing tonic spiking. With the first parameter set (model A), increasing g_{Ca} (Ab) or g_{BK} (Ac) by 1 nS does not affect the tonic spiking. With the second parameter set (model B), increasing g_{BK} (Bc) results in a transition to bursting, but increasing g_{Ca} (Bb) does not. Using the third parameter set (model C), an increase in g_{Ca} (Cb) results in a transition to bursting, but an increase in g_{BK} (Cc) does not.

TABLE 2 Parameter values used for Fig. 1

	g_{Ca}	g_K	g_{SK}	g_{BK}	g_{leak}
Model A	2.36	5.64	3.14	1.91	0.16
Model B	3.80	5.57	3.13	2.06	0.29
Model C	2.38	4.08	2.61	0.15	0.24

All conductance values are expressed in nS.

changes in one or more conductance. Therefore, predictions made for the different individuals (e.g., that increasing Ca^{2+} conductance should convert tonic spiking to bursting) would be different. If tested on an actual cell, the outcome of the test would depend on how well the dynamical properties of the chosen cell match those of the individual used to make the prediction. Our goal is to build a cellular model such that the actual cell and the model are in similar regions of parameters space, so they react similarly to parameter changes.

A new process for model building and testing

The typical process for model building and testing begins with data collection, often from experiments performed on several cells (Fig. 2 A, cells A, B, C, etc.), and often from different laboratories. The collected data represent a patchwork of results describing the behavior of a cell type, and they are compiled into a model. The model usually reflects the properties of an average or representative cell, assuming all the caveats associated with average/representative models (6,10,27). Once a calibrated model is developed, one or more predictions are generated. In the example in Fig. 2 the prediction is that an increase in the maximal BK conductance will change the cell's electrical activity from tonic spiking to bursting. Finally, predictions generated by the model are experimentally tested. This testing is done on cells other than those used to develop and calibrate the model. Even if the model's activity resembles the activity of the cells used to test its predictions, it may correspond to a different location in parameter space and thus react differently to conductance changes (Fig. 1).

Fig. 2 B illustrates our strategy for performing model calibration and testing on the same cell. Before an experiment is begun, a mathematical model is built, and parameter values are set using available data. Parameters of the most interest are then identified, either by a sensitivity analysis of the model, or based on previously recorded experimental data. These parameters of interest (typically the maximal conductances) are then subject to individual-cell calibration using
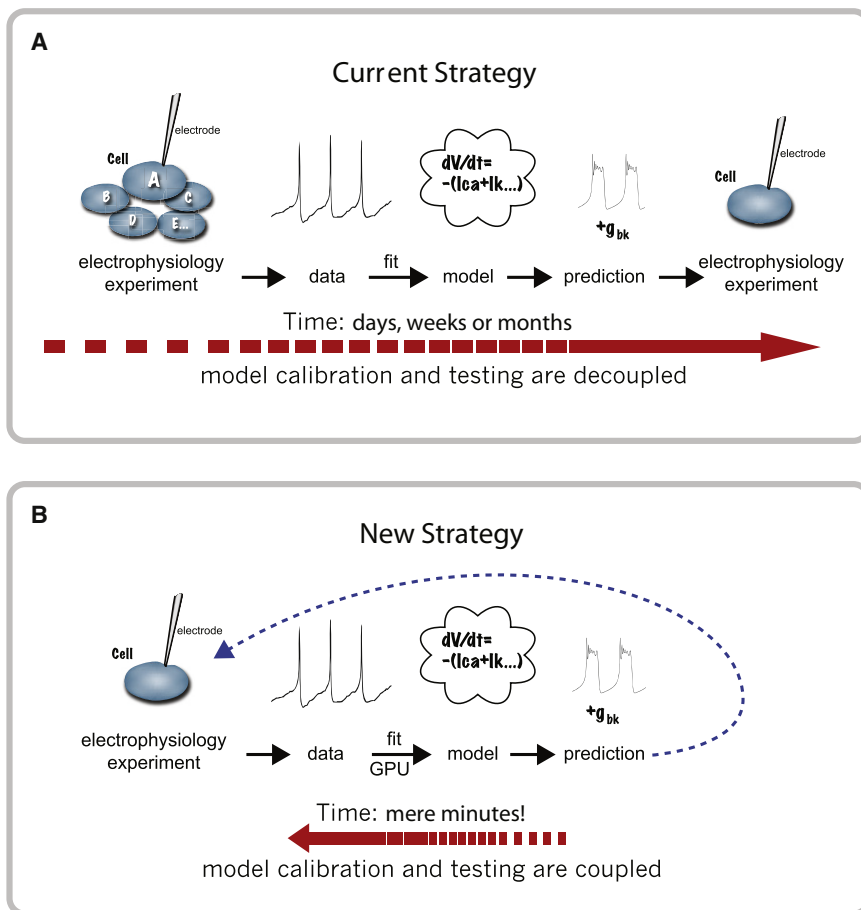

FIGURE 2 Current and new strategies for model calibration and predictions testing. (A) With the current strategy, a model is tested on cells other than those used for calibration. (B) With the new strategy, the model is tested on the cell used to calibrate it.

a recording of the cell's spontaneous electrical activity, as discussed in Materials and Methods. This calibration focuses on features of the voltage trace, such as period or burst duty cycle, rather than on the noisy voltage time course itself. The calibration can be done in ~10 min using a GPU, which can run thousands of numerical simulations simultaneously. The same process using a standard processor would take approximately 20–30 times longer, depending on the computer. When a best fit is found, predictions are generated with this model and tested on the same cell used to do the model calibration. A key element of this process is the rapid optimization done with the GPU, since it can be completed while the cell is still healthy.

Model calibration on synthetic data

Before illustrating the procedure with actual data, we examine how fitting features of the voltage trace constrains model parameters. That is, we determine how well we can retrieve correct parameters using a fitting procedure based on fitting features of the voltage trace, as well as fitting current under voltage clamp. This is done with simulated or synthetic data, since in this case the values of all parameters used to generate the data are known. We consider the calibration on two different types of simulated electrical activity, tonic spiking and fast bursting, both of which are common types of electrical activity in anterior pituitary cells.

We first simulate the electrical activity using a reference parameter set and extract the features that will represent the set of target features. We then use Latin hypercube sampling to generate 4096 model cells, with different values of the maximal conductances g_{Ca}, g_K, g_{SK}, g_{BK}, and g_{leak}. We perform up to 10 generations of optimization to find values for these parameters that best fit the features of the reference voltage trace, as discussed in Materials and Methods. The reference parameter sets used to generate spiking and bursting are in Table 1 (default values). Spiking was produced using a low BK conductance ($g_{BK} = 0.1$ nS), and bursting was produced using a larger value ($g_{BK} = 0.8$ nS).

We examine the proximity of the best-fit parameters to the target parameters used to produce the synthetic spiking or bursting data. We define a distance measure as $(p_i - p_T)/p_T$, where p_i is the estimated parameter and p_T is the target value for that parameter. This measure is then the fractional deviation from the target value. A value close to zero signifies almost perfect accuracy, and a value of 1 signifies that the parameter estimated is 100% different from the value of the target parameter.

Fig. 3 shows best-fit solutions for tonic spiking and bursting. Fig. 3 A shows that the best-fit voltage trace completely overlaps that of the target spiking trace; the voltage-clamp currents match very closely (Fig. 3 B) and the parameter distances from the targets (Fig. 3 C) are minimal. The fit is as good and the parameter distances
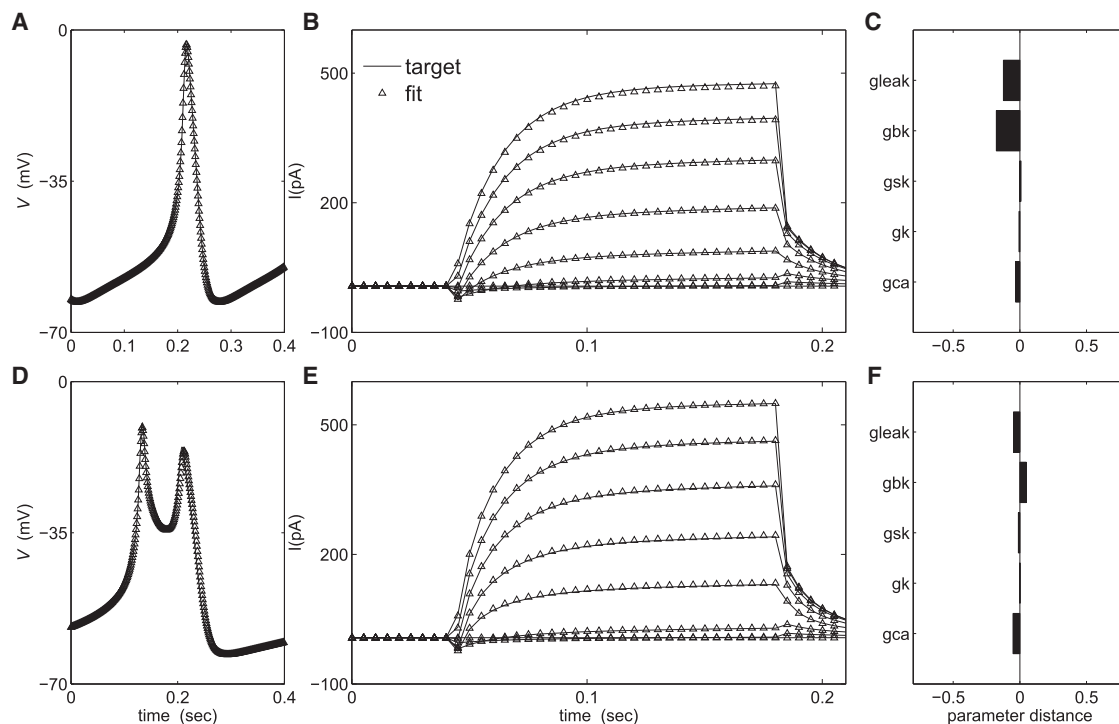

FIGURE 3 Calibration on synthetic data. (A and D) Target trace (*solid line*) and corresponding fit (*open triangles*) for tonic spiking (A) and bursting (D). (B and E) Target voltage-clamp currents (*solid lines*) and corresponding fits (*open triangles*) for tonic spiking (B) and bursting (E). (C and F) Parameter distances for spiking (C) and bursting (F).

between the best-fit and target parameters are even smaller in the case of a bursting model cell (Fig. 3, *D–F*). This shows that the process of calibrating a model using features of the voltage trace and voltage-clamp data can yield parameter combinations that successfully reproduce a target voltage trace. Few generations are needed, because at each generation we sample a wide region of the parameter space using the parallel computational capabilities of the GPU.

We summarize the performance of the calibration process for the spiking and bursting cells, with and without voltage clamp, in Fig. 4. This figure shows, for the best-fit cell, the fitness and the sum of the average absolute parameter distances for the five parameters used in the fitting. The parameter values for the best-fit bursting model cell are closer to the targets (Fig. 4 *B*, *second and fourth bars*) than those for the spiking cell (Fig. 4 *B*, *first and third bars*), since the bursting pattern is more complex than the spiking pattern, which places more constraints on the parameters. The addition of voltage-clamp data to the calibration process, as well as voltage-trace features, results in a marginal improvement of the fit to the voltage trace (Fig. 4 *A*), but a great improvement in the accuracy of the parameter estimation (Fig. 4 *B*).

We next consider the relation between the number of parameters to be estimated and the accuracy in estimating them. First, we select the number, *N*, of parameters to be estimated. We then randomly pick *N* parameters from all the available model parameters. For each parameter chosen, we define a search space within $\pm 90\%$ of the default value for that parameter. We then run the calibration process for 10 generations and retain the best-fit model. The process

is repeated 10 times for each *N*. Synthetic bursting activity was used as a target.

The results show, not surprisingly, that as the number of parameters increases the quality of the fit decreases and the accuracy in parameter estimation decreases. The impact of increasing parameter number on the fit to the features (Fig. 4 *C* (vertical axis starts at 0.85)) is much less than the impact on the accuracy of the parameter estimation (Fig. 4 *D*). However, even when 10 parameters are fit, the mean parameter distance is only 0.4. Of course, different parameters have different impacts on the behavior of the system, as could be deduced by a sensitivity analysis. Parameters with low sensitivity will be harder to estimate than those with high sensitivity, but errors in these parameters will have less impact on qualitative predictions.

Comparing predictive expectations

A model, however sophisticated, will never be exactly like a real cell. There are channels and other cell components not included in the model, and those components that are included have varying degrees of simplification. The calibrated parameters will thus never be absolutely correct. However, what matters most is that the model be complete enough to make nontrivial, testable predictions. Here, we examined whether the calibration process estimates parameter values sufficiently well that testable predictions can be made.

We first established a way to compare how distinct models differ in their ability to generate correct predictions.
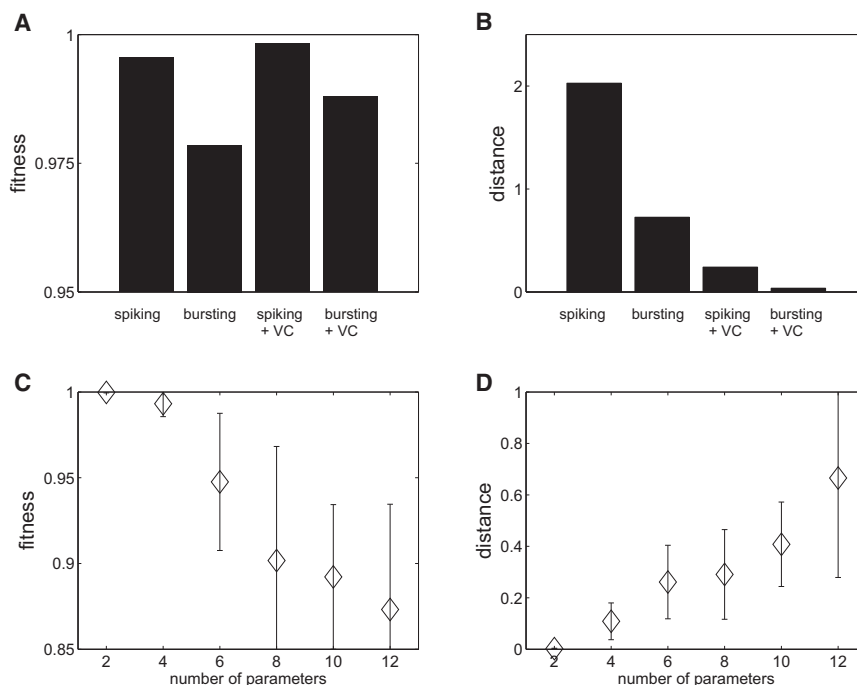
FIGURE 4 Accuracy of calibration depends on the data used and the number of fitting parameters. Each column represents the average of 10 fits. (*A*) Average fitness score for fits to tonic spiking, bursting, spiking using voltage-clamp (VC) data, and bursting using voltage-clamp data. (*B*) The average parameter distance (sum of the absolute distances for the five fitting parameters) is greatly reduced when voltage-clamp data are used in the fitting process. (*C* and *D*) Fitness and parameter accuracy decline as the number of free parameters is increased. For all fits, we used bursting with voltage-clamp data. Each data point represents the mean of 10 fits, with randomly chosen parameters to be estimated. For each parameter we created a uniform distribution within $\pm 90\%$ of its default value. (*C*) Fitness decreases as the number of parameters increases. (*D*) Accuracy of parameter estimation decays (absolute parameter distance increases) as the number of parameters to be estimated increases.

For each of the six parameters (g_{Ca}, g_K, g_{SK}, g_{BK}, g_{leak}, and τ_{BK}), we increased its value by 50% in 40 simulated model cells, and then determined whether the perturbation resulted in a qualitative change of the electrical activity and if so, of which nature (i.e., spiking to bursting, bursting to spiking, or active to silent). This generated an array containing the values of the qualitative changes for each perturbation in each model cell, which we refer to as the predictive set. The predictive set of the model cell used to produce synthetic data (the target cell) can be compared with those of fitted cells to determine the ability of the fitting process to make correct predictions. The best possible case is that of a calibrated model for which all six perturbations result in a correct prediction. We considered several possible scenarios to assess the predictive ability of the model with the calibration procedure. For each scenario, we scored the percentage of times when at least two, four, or all six predictions were correct.

Scenario 1: No calibration

In the case of a tonically spiking target cell, we compared its predictive set with the predictive set obtained by averaging >20 models, each with five randomly chosen parameters (g_{Ca}, g_K, g_{SK}, g_{BK}, and g_{leak}), that exhibited tonic spiking. A similar procedure was applied in the case of a bursting target cell. These tests on uncalibrated models enable us to establish a baseline for comparison with calibrated models. The resulting set of predictions (Fig. 5 A CTRL) shows that only about one-third of uncalibrated models can make 2/6 correct predictions (mean, $\mu = 0.3$; standard deviation, $\sigma = 0.46$).

Scenario 2: Full calibration

The predictive sets of 40 target cells were compared to the predictive sets of calibrated models with the same free parameters as in the first scenario. In this case, the average percentage of correct predictions (Fig. 5 A, Calibration) is much higher than in the case of predictions made with the uncalibrated models. About 75% of calibrated models make 6/6 correct predictions.

Scenario 3: Missing current

In 40 target cells, we added a fast-inactivating A-type K^+ current, I_A, which is known to be present in some pituitary cells [28] and can regulate the transition between spiking and bursting [15,29]. The I_A current is described by the equations

$$I_A = g_A a_\infty(V) h(V - V_k), \qquad (10)$$

with inactivation variable h satisfying

$$\tau_h \frac{dh}{dt} = h_\infty(V) - h, \qquad (11)$$

where

$$h_\infty(V) = \left[1 + exp\left(\frac{(v - v_h)}{s_h}\right)\right]^{-1} \qquad (12)$$

and

$$a_\infty(V) = \left[1 + exp\left(\frac{(v_a - v)}{s_a}\right)\right]^{-1}. \qquad (13)$$
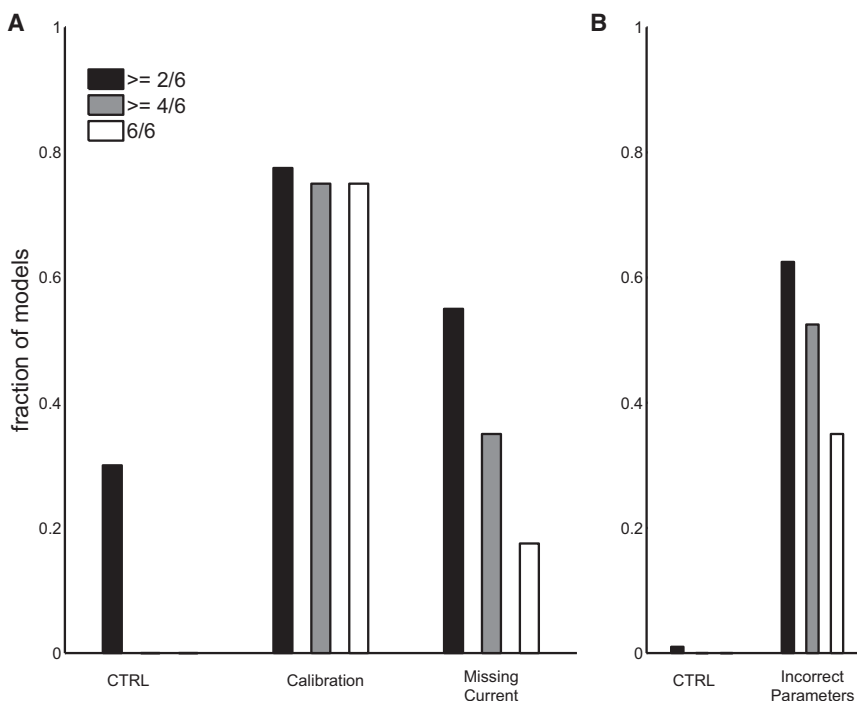

FIGURE 5 Predictions using different calibration scenarios. The vertical axis shows the fraction of models with ≥ 2 (black), ≥ 4 (gray), and 6 (white bars) of 6 correct predictions. (A) First set of bars (CTRL) is for the case where no calibration was used. Second set of bars (Calibration) shows the case where the calibration process was used to fit five parameters. Third set of bars (Missing Current) refers to the case where calibration was used to fit five parameters but a current was missing from the model. (B) CTRL bars refer to no calibration, and all parameters were different from the target. Second set of bars (Incorrect Parameters) refers to the case where the calibration procedure was used to fit five parameters.

In all target cells, g_A was set to 20 nS. We then ran the calibration process on each of the selected cells, but without including the added current. This scenario tests how well predictions can be made even if the model lacks an ionic current that is present in the cell. A significant fraction of models were able to make some correct qualitative predictions. However, the fraction of models making more than 4/6 correct predictions is considerably reduced in this scenario (Fig. 5 A, *Missing Current*).

Scenario 4: Incorrect parameters

We ran the calibration process using five calibration parameters (g_{Ca}, g_K, g_{SK}, g_{BK}, and g_{leak}) after introducing changes to all the other parameters (each is subject to a random change of ±10% of its value). The baseline for comparison (the control) was generated as in Scenario 1: if the model cell was spiking (or bursting), we compared its predictive set with the predictive set obtained by averaging >20 randomly chosen model cells exhibiting tonic spiking (or bursting), where each control cell had the same set of incorrect parameters as the set of calibrated cells. Fig. 5 B (*CTRL*) shows that, with these uncalibrated test cells, very few predictions match the prediction set of the target cells. Thus, although the test cells match the spontaneous behaviors of the target cells, they lead almost uniformly to invalid predictions. When the calibration procedure was applied to the test cells (calibrating five parameters), the results were much improved (Fig. 5 B, *Incorrect Parameters*). This

shows that even if none of the parameter values matches those of the targets, the model can be predictive if the calibration procedure is applied to a subset of the parameters.

Experimental test of the calibration procedure

Here, we provide some examples of the calibration procedure used in experimental settings. We focus our attention on the modulatory effect of the BK current, since it is important for determining whether a cell is spiking or bursting (25,30,31). The dynamic-clamp technique is used to inject an artificial BK current into the cell, as described in Materials and Methods.

Spiking to bursting

In the first experiment, we considered the transition from spiking to bursting (Fig. 6, *A–D*). We asked whether addition of a BK-type current could result in a spiking-to-bursting transition, and if so, what BK maximal conductance would be needed. The experimental cell exhibited spontaneous electrical activity, with spiking and bursting interspersed (not shown). A pharmacological agent was administered that irreversibly blocks the activity of BK channels (paxilline, 1 μM), and a few minutes later the cell displayed tonic spiking (Fig. 6 B, *solid trace*). This suggests that the BK current was responsible for the bursting mixed in with the spiking in the cell's spontaneous activity.
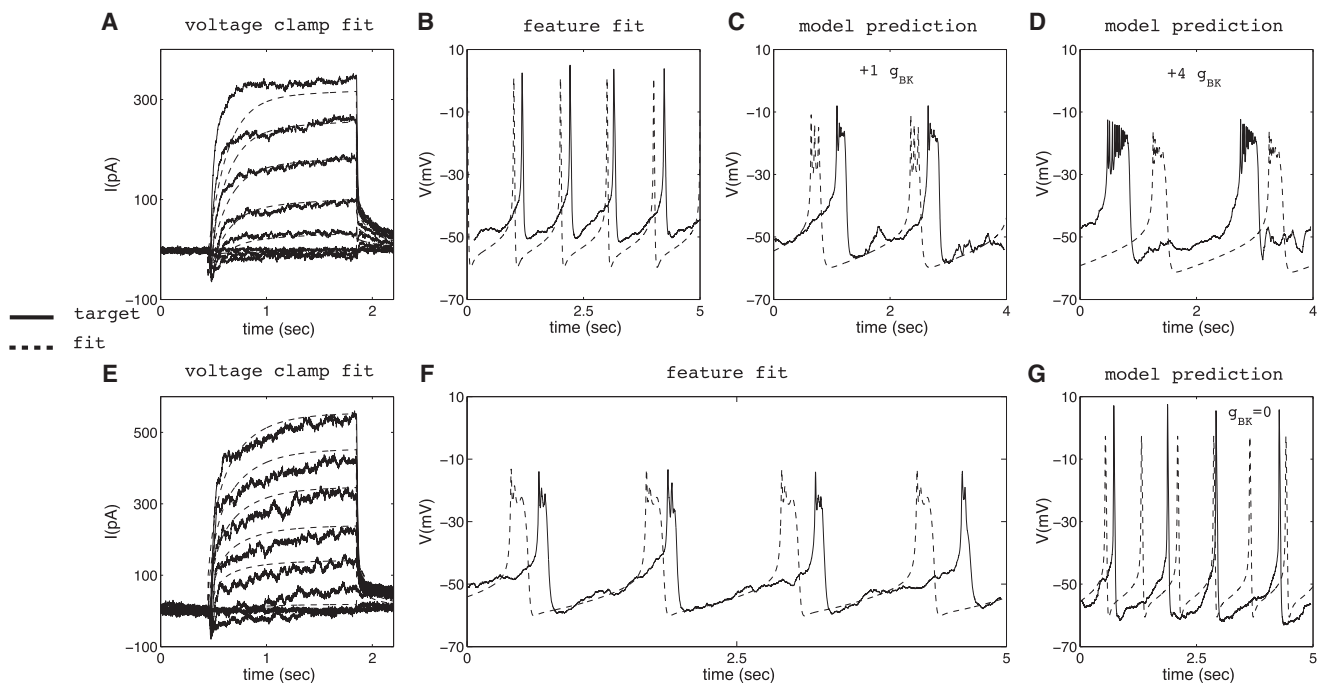

FIGURE 6 Testing model predictions: bursting from spiking and vice versa via BK modulation. (*A and B*) Voltage-clamp and voltage-trace model fits. (*C*) Testing the model prediction (*dashed line*) that adding 1 nS of BK conductance should convert spiking to bursting. Tested on the same cell used for calibration (*solid line*). (*D*) Testing the model prediction that a further increase in BK conductance will increase the duration of the burst active phase. (*E and F*) Voltage-clamp and voltage-trace model fits. (*G*) Testing the model prediction that removal of BK conductance should convert bursting to spiking.

With paxilline present, a few minutes of spiking activity were recorded and the features were extracted from the voltage trace. These features and the recorded voltage-clamp protocol (Fig. 6 A, *solid trace*) were used as a target for the calibration procedure (with nine calibration parameters: C, v_m, s_m, g_{Ca}, g_K, τ_n, g_{SK}, g_{leak}, and V_{leak}), with the maximal conductance of the BK current (g_{BK}) set to zero. The best-fit model reproduces the period and the mean spike amplitude (Fig. 6 B, *dashed trace*), as well as the steady-state currents under voltage clamp (Fig. 6 A, *dashed trace*). Using the model cell, we generated predictions about the effects of adding back a BK with a range of maximum conductances. Simulations of the model cell predicted that addition of BK current would recover bursting with the transition occurring at g_{BK} = 0.5 nS. Further increases of g_{BK} resulted in increasing durations of the burst active phase with little effect on the burst period. We tested these predictions on the same cell using the dynamic clamp. The onset of bursting was first observed when we injected 0.5 nS of BK current (results not shown), and it was mixed with spiking activity. When the BK current injected was increased to 1 nS the bursting activity was consolidated (Fig. 6 C, *solid trace*). Simulations with the model cell accurately predicted the burst period, the burst amplitude, and the burst duration relative to the silent phase (Fig. 6 C, *dashed trace*). The model predicted that when the BK conductance was increased to 4 nS, there would be an increase in the active-phase duration with little change in burst period (Fig. 6 D, *dashed trace*). This was verified when the BK conductance added to the actual cell was increased to 4 nS (Fig. 6 D, *solid trace*).

Bursting to spiking

In this experiment, we considered the transition from bursting to spiking. We recorded the electrical activity from a cell displaying bursting with a period of ~0.6 s (Fig. 6 F, *solid trace*) and used the voltage-trace features and the voltage-clamp data (Fig. 6 E, *solid trace*) to run the calibration process. We then asked whether subtraction of the estimated BK conductance in the calibrated cell would result in a transition from bursting to spiking. Finally we tested the prediction in the experimental cell.

The calibration procedure (10 free parameters: C, v_m, s_m, g_{Ca}, g_K, g_{BK}, τ_n, g_{SK}, g_{leak}, and V_{leak}) resulted in a model cell that was consistent with the voltage-clamp data (Fig. 6 E, *dashed trace*) and the bursting activity (Fig. 6 F, *dashed trace*). With this calibrated model cell, it is predicted that removing the BK conductance (estimated at g_{BK} = 1.52 nS) should switch the electrical activity from bursting to spiking (Fig. 6 G, *dashed trace*). We tested this prediction in the same cell by bath application of the BK blocker paxilline (1 μM), and, as predicted, the cell displayed tonic spiking (Fig. 6 G, *solid trace*).

Interaction between the BK conductance and the BK-channel time constant

In this experiment, we explored how the transition from bursting to spiking is affected by changes to both g_{BK} and the time constant of BK-channel activation (τ_{BK}). We previously demonstrated that the ability of a BK current to promote bursting depends on the magnitude of the BK conductance and on the BK-channel activation rate (31). If this activation is not fast enough, the BK current no longer promotes bursting.

We recorded the electrical activity from a cell that exhibits spontaneous tonic spiking (Fig. 7, *data*) and used part of this trace to compute the features for the calibration procedure (eight calibration parameters: C, g_{Ca}, g_K, g_{SK}, g_{BK}, k_c, g_{leak}, and V_{leak}). The resulting calibrated cell (Fig. 7, *model*) matches the period, the shape of the action potential, and the mean amplitude of the experimental cell. Using the model, we explored 1), whether a BK current could promote bursting, and 2), the effect of increasing the BK conductance and the time constant of the BK channel activation. Simulations predicted that the transition to bursting occurs for g_{BK} = 0.2 nS and bursting persists if g_{BK} is increased to 1 nS (Fig. 7, prediction 1). When g_{BK} and τ_{BK} are increased to 10 nS and 10 ms, respectively, the model predicts that the duration of the burst active phase should increase, whereas the amplitude should decrease (Fig. 7, prediction 2). Finally, when τ_{BK} is increased from 10 to 13 ms, the same addition of BK current (g_{BK} = 10 nS) does not convert spiking to bursting (Fig. 7, prediction 3).

We tested these predictions with the dynamic clamp on the cell used to calibrate the model. The transition to bursting was observed when 0.4 nS of BK conductance was injected (results not shown), as well as when g_{BK} = 1 nS was added (Fig. 7, test 1). Different values of g_{BK} were tested (1, 2, 4, 10, 25, and 100 nS), and bursting oscillations were observed in all cases (results not shown). The value of g_{BK} = 10 nS was chosen to investigate the effect of the time constant of BK-channel opening. Using g_{BK} =10 nS, when the value of τ_{BK} was increased from 5 to 10 ms, the burst active phase was increased and the amplitude decreased, as predicted (Fig. 7, test 2). With a longer time constant of τ_{BK} = 12 ms, the addition of BK current did not convert the spiking to bursting (Fig. 7, test 3), again consistent with the prediction.

We have evaluated our procedure on six cells so far, for a total of 30 predictions regarding BK and K conductances. Using calibrated models, the percentage of correct predictions (87%) was higher than the percentage of correct predictions using random noncalibrated models (44%).

DISCUSSION

We have presented an approach for confronting heterogeneity in a cell population, wherein we calibrate a model
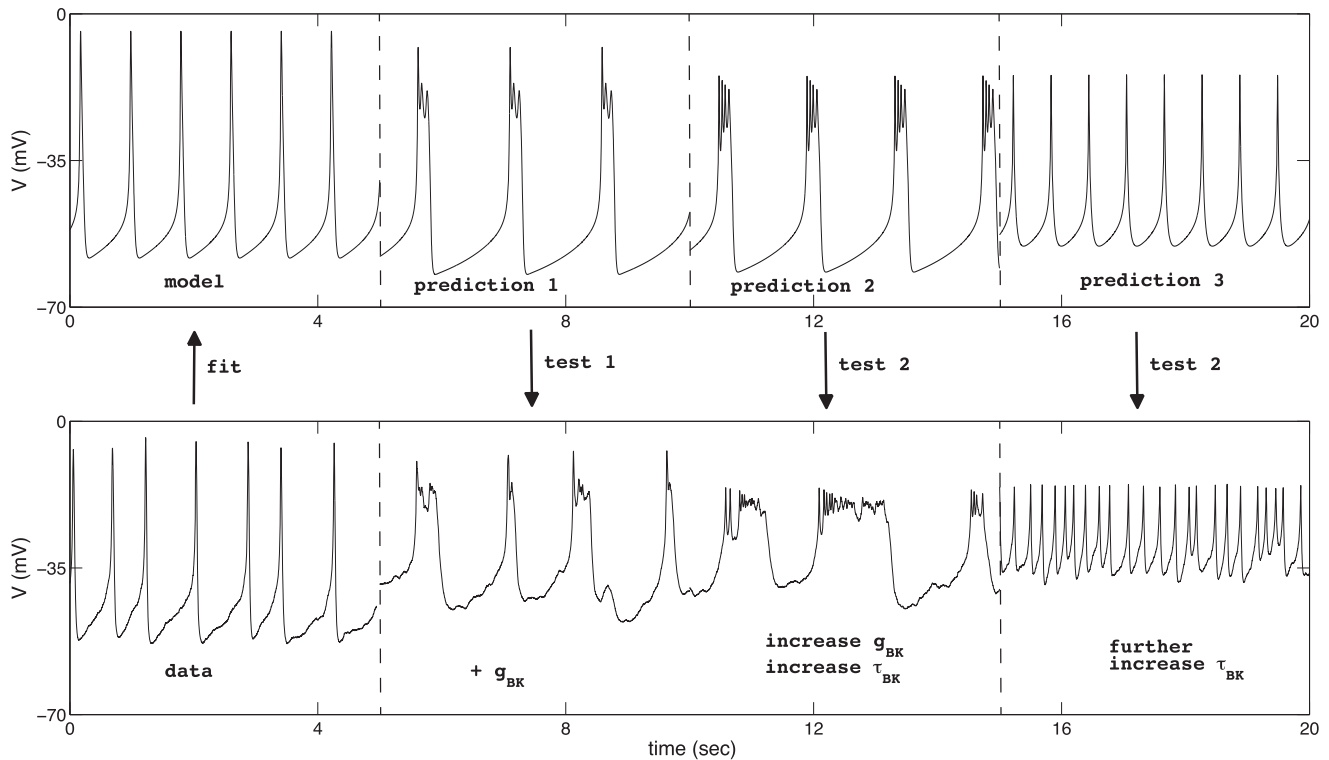
FIGURE 7   The model was calibrated to a spiking cell and then several predictions were made and tested with dynamic clamp on the same cell. Prediction 1 was that spikes would convert to bursting when $g_{BK} = 1$ nS is added. Prediction 2 was that broadening of the active phase and reduction of amplitude would occur when g_{BK} is 10 nS and τ_{BK} is increased to 10 ms. Prediction 3 was that there would be no conversion to bursting when τ_{BK} is 12 ms or more in the added current. The dashed lines indicate breaks in time.

using a single cell and test predictions on that same cell. This has similarities to the approach of Hobbs and Hooper (32), but with our approach the model parameters are estimated while the cell is still being recorded. The speed with which we can find a combination of parameters to match the cell's activity allows us to test the model on that very same cell.

The fast calibration speed is achieved by using a programmable GPU to inexpensively parallelize computations, and prediction testing is performed using the dynamic-clamp method. The cost to equip a laboratory with these tools is low, ~5–10% of the price of a patch-clamp setup. Most modern computers come equipped with one GPU, and more can be added; with several GPU units, one could test populations of models with different current combinations. Given these advantages, GPUs are becoming increasingly important in computational biology (33,34).

The number of parameters that can be estimated from noisy data is always limited. Here, we have used a feature-based estimation method (19), because directly fitting a noisy voltage trace is not necessary or desirable. To further constrain parameter values, we have also used voltage-clamp recordings of whole-cell currents. Nevertheless, there is a limit on the number of parameters we can estimate, which places a limit on the level of detail achievable in the model. A possible improvement would be to use

wide-dynamic-range voltage-clamp signals (32). Although this could improve the number of parameters we can estimate, there will always be a limit, and a model is always a simplification of the biological system. Thus, we cannot expect to find a unique set of parameters that represents the single cell being studied.

Instead, we seek to develop a model that shares the essential dynamical properties with the cell being investigated. This means that the change in the activity pattern of the model should be qualitatively similar to the change of the cell's pattern when key parameters, such as maximal conductances, are varied. Here, we looked at the effects of the BK conductance, which has been our recent focus (31). We showed that the models obtained from spiking cells could be converted to bursting with the addition of BK conductance, and using the dynamic-clamp method, we verified these predictions on the same cells that were used to produce the models. We have also shown (using synthetic data) that even if our model does not contain all the conductances present in the cell, it can still produce correct qualitative predictions.

Using this, to our knowledge, new approach it is possible to assemble a population of models, each representing a single individual in a heterogeneous cell population. Each model can be validated using the cell from which it was derived. The ensemble of model cells can then be

used to examine the source of heterogeneity in the population and the effects of heterogeneity on the behavior of the population in response to stimuli.

REFERENCES

1. Winiger, B. P., F. Wuarin, ..., W. Schlegel. 1987. Single cell monitoring of cytosolic calcium reveals subtypes of rat lactotrophs with distinct responses to dopamine and thyrotropin-releasing hormone. *Endocrinology.* 121:2222–2228.

2. Lledo, P. M., N. Guerineau, ..., J. M. Israel. 1991. Physiological characterization of two functional states in subpopulations of prolactin cells from lactating rats. *J. Physiol.* 437:477–494.

3. Tomaiuolo, M., R. Bertram, ..., J. Tabak. 2010. Investigating heterogeneity of intracellular calcium dynamics in anterior pituitary lactotrophs using a combined modelling/experimental approach. *J. Neuroendocrinol.* 22:1279–1289.

4. Horta, J., M. Hiriart, and G. Cota. 1991. Differential expression of Na channels in functional subpopulations of rat lactotropes. *Am. J. Physiol.* 261:C865–C871.

5. Goldman, M. S., J. Golowasch, ..., L. F. Abbott. 2001. Global structure, robustness, and modulation of neuronal models. *J. Neurosci.* 21:5229–5238.

6. Golowasch, J., M. S. Goldman, ..., E. Marder. 2002. Failure of averaging in the construction of a conductance-based neuron model. *J. Neurophysiol.* 87:1129–1131.

7. Marder, E., and A. L. Taylor. 2011. Multiple models to capture the variability in biological neurons and networks. *Nat. Neurosci.* 14:133–138.

8. Sherman, A. 2011. Dynamical systems theory in physiology. *J. Gen. Physiol.* 138:13–19.

9. Prinz, A. A., D. Bucher, and E. Marder. 2004. Similar network activity from disparate circuit parameters. *Nat. Neurosci.* 7:1345–1352.

10. Foster, W. R., L. H. Ungar, and J. S. Schwaber. 1993. Significance of conductances in Hodgkin-Huxley models. *J. Neurophysiol.* 70:2502–2518.

11. Van Goor, F., D. Zivadinovic, ..., S. S. Stojilkovic. 2001. Dependence of pituitary hormone secretion on the pattern of spontaneous voltage-gated calcium influx. Cell type-specific action potential secretion coupling. *J. Biol. Chem.* 276:33840–33846.

12. Prinz, A. A., L. F. Abbott, and E. Marder. 2004. The dynamic clamp comes of age. *Trends Neurosci.* 27:218–224.

13. Sharp, A. A., M. B. O'Neil, ..., E. Marder. 1993. Dynamic clamp: computer-generated conductances in real neurons. *J. Neurophysiol.* 69:992–995.

14. Nowotny, T., A. Szücs, ..., A. I. Selverston. 2007. Models wagging the dog: are circuits constructed with disparate parameters? *Neural Comput.* 19:1985–2003.

15. Tabak, J., N. Toporikova, ..., R. Bertram. 2007. Low dose of dopamine may stimulate prolactin secretion by increasing fast potassium currents. *J. Comput. Neurosci.* 22:211–222.

16. Fakler, B., and J. P. Adelman. 2008. Control of K(Ca) channels by calcium nano/microdomains. *Neuron.* 59:873–881.

17. Simon, S. M., and R. R. Llinás. 1985. Compartmentalization of the submembrane calcium activity during calcium influx and its significance in transmitter release. *Biophys. J.* 48:485–498.

18. Sherman, A., J. Keizer, and J. Rinzel. 1990. Domain model for Ca^{2+}-inactivation of Ca^{2+} channels at low channel density. *Biophys. J.* 58:985–995.

19. Ermentrout, G. B. 2002. Simulating, Analyzing, and Animating Dynamical Systems: A Guide to XPPAUT for Researchers and Students. SIAM, Philadelphia.

20. Druckmann, S., Y. Banitt, ..., I. Segev. 2007. A novel multiple objective optimization framework for constraining conductance-based neuron models by experimental data. *Front. Neurosci.* 1:7–18.

21. McKay, M. D., W. J. Conover, and R. J. Beckman. 1979. A comparison of three methods for selecting values of input variables in the analysis of output from a computer code. *Technometrics.* 42:55–61.

22. Tashjian, Jr., A. H., Y. Yasumura, ..., M. L. Parker. 1968. Establishment of clonal strains of rat pituitary tumor cells that secrete growth hormone. *Endocrinology.* 82:342–352.

23. Milescu, L. S., T. Yamanishi, ..., J. C. Smith. 2008. Real-time kinetic modeling of voltage-gated ion channels using dynamic clamp. *Biophys. J.* 95:66–87.

24. Prinz, A. A., C. P. Billimoria, and E. Marder. 2003. Alternative to hand-tuning conductance-based models: construction and analysis of databases of model neurons. *J. Neurophysiol.* 90:3998–4015.

25. Van Goor, F., Y.-X. Li, and S. S. Stojilkovic. 2001. Paradoxical role of large-conductance calcium-activated K^+ (BK) channels in controlling action potential-driven Ca^{2+} entry in anterior pituitary cells. *J. Neurosci.* 21:5902–5915.

26. Gonzalez-Iglesias, A. E., Y. Jiang, ..., S. S. Stojilkovic. 2006. Dependence of electrical activity and calcium influx-controlled prolactin release on adenylyl cyclase signaling pathway in pituitary lactotrophs. *Mol. Endocrinol.* 20:2231–2246.

27. Golowasch, J., L. F. Abbott, and E. Marder. 1999. Activity-dependent regulation of ionic currents in an identified neuron of the stomatogastric ganglion of the crab *Cancer borealis. J. Neurosci.* 19:31–35.

28. Chung, S., D. B. Saal, and L. K. Kaczmarek. 1995. Elimination of potassium channel expression by antisense oligonucleotides in a pituitary cell line. *Proc. Natl. Acad. Sci. USA.* 92:5955–5959.

29. Toporikova, N., J. Tabak, ..., R. Bertram. 2008. A-type K^+ current can act as a trigger for bursting in the absence of a slow variable. *Neural Comput.* 20:436–451.

30. Tsaneva-Atanasova, K., A. Sherman, ..., S. S. Stojilkovic. 2007. Mechanism of spontaneous and receptor-controlled electrical activity in pituitary somatotrophs: experiments and theory. *J. Neurophysiol.* 98:131–144.

31. Tabak, J., M. Tomaiuolo, ..., R. Bertram. 2011. Fast-activating voltage- and calcium-dependent potassium (BK) conductance promotes bursting in pituitary cells: a dynamic clamp study. *J. Neurosci.* 31:16855–16863.

32. Hobbs, K. H., and S. L. Hooper. 2008. Using complicated, wide dynamic range driving to develop models of single neurons in single recording sessions. *J. Neurophysiol.* 99:1871–1883.

33. Clayton, T. F., A. F. Murray, and G. Leng. 2010. Modelling the in vivo spike activity of phasically-firing vasopressin cells. *J. Neuroendocrinol.* 22:1290–1300.

34. Ben-Shalom, R., A. Aviv, ..., A. Korngreen. 2012. Optimizing ion channel models using a parallel genetic algorithm on graphical processors. *J. Neurosci. Methods.* 206:183–194.